

DTIC FILE COPY

4

AD-A213 901

Nighttime Na-D Emission Observed from a Polar Orbiting DMSP Satellite

A. L. NEWMAN
Space Sciences Laboratory
Laboratory Operations
The Aerospace Corporation
El Segundo, CA 90245

1 September 1989

Prepared for

SPACE SYSTEMS DIVISION
AIR FORCE SYSTEMS COMMAND
Los Angeles Air Force Base
P.O. Box 92960
Los Angeles, CA 90009-2960

DTIC
ELECTE
OCT 27 1989
S E D

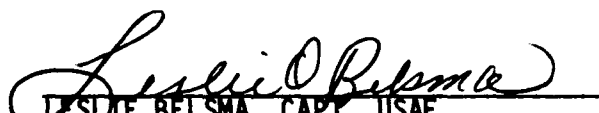
APPROVED FOR PUBLIC RELEASE;
DISTRIBUTION UNLIMITED


89 10 27 096

This report was submitted by The Aerospace Corporation, El Segundo, CA 90245, under Contract No. F04701-85-C-0086-P00016 with the Space Systems Division, P.O. Box 92960, Los Angeles, CA 90009-2960. It was reviewed and approved for The Aerospace Corporation by H. R. Rugge, Director, Space Sciences Laboratory. Capt Leslie Belsma, SSD/DAAX, was the project officer for the Mission-Oriented Investigation and Experimentation (MOIE) Program.

This report has been reviewed by the Public Affairs Office (PAS) and is releasable to the National Technical Information Service (NTIS). At NTIS, it will be available to the general public, including foreign nationals.

This technical report has been reviewed and is approved for publication. Publication of this report does not constitute Air Force approval of the report's findings or conclusions. It is published only for the exchange and stimulation of ideas.


LESLIE BELSMA, CAPT, USAF
MOIE Project Officer
SSD/DAAX


JAMES A. BERES, LT COL, USAF
MOIE Program Manager
AFSTC/WCO OL-AB

REPORT DOCUMENTATION PAGE

1a. REPORT SECURITY CLASSIFICATION Unclassified			1b. RESTRICTIVE MARKINGS	
2a. SECURITY CLASSIFICATION AUTHORITY			3. DISTRIBUTION/AVAILABILITY OF REPORT Approved for public release; distribution unlimited.	
2b. DECLASSIFICATION/DOWNGRADING SCHEDULE				
4. PERFORMING ORGANIZATION REPORT NUMBER(S) TR-0086A(2940-04)-2			5. MONITORING ORGANIZATION REPORT NUMBER(S) SD-TR-89-62	
6a. NAME OF PERFORMING ORGANIZATION The Aerospace Corporation Laboratory Operations		6b. OFFICE SYMBOL (If applicable)		7a. NAME OF MONITORING ORGANIZATION Space Systems Division
6c. ADDRESS (City, State, and ZIP Code) El Segundo, CA 90245			7b. ADDRESS (City, State, and ZIP Code) Los Angeles Air Force Base Los Angeles, CA 90009-2960	
8a. NAME OF FUNDING/SPONSORING ORGANIZATION		8b. OFFICE SYMBOL (If applicable)		9. PROCUREMENT INSTRUMENT IDENTIFICATION NUMBER F04701-85-C-0086-P00016
8c. ADDRESS (City, State, and ZIP Code)			10. SOURCE OF FUNDING NUMBERS	
			PROGRAM ELEMENT NO.	PROJECT NO.
			TASK NO.	WORK UNIT ACCESSION NO.
11. TITLE (Include Security Classification) Nighttime Na-D Emission Observed from a Polar Orbiting DMSP Satellite				
12. PERSONAL AUTHOR(S) Newman, Alice L.				
13a. TYPE OF REPORT		13b. TIME COVERED FROM _____ TO _____		14. DATE OF REPORT (Year, Month, Day) 1989 September 1
15. PAGE COUNT 34				
16. SUPPLEMENTARY NOTATION				
17. COSATI CODES			18. SUBJECT TERMS (Continue on reverse if necessary and identify by block number)	
FIELD	GROUP	SUB-GROUP	<input checked="" type="checkbox"/> Airglow <input checked="" type="checkbox"/> Ozone <input checked="" type="checkbox"/> Global <input checked="" type="checkbox"/> Sodium <input checked="" type="checkbox"/> Nightglow	
19. ABSTRACT (Continue on reverse if necessary and identify by block number)				
<p>Limb scans of nighttime sodium doublet emissions at 589 nm were performed globally from a sun-synchronous satellite during July 1979. The observations have provided a global description of variations in the emitting layer with latitude and altitude. The limb-scan data are consistent with the presence of a 10 km thick emitting layer near the 90 km peak of the sodium density in the northern midlatitude mesosphere in summer. At equatorial and southern latitudes, however, a narrower emission layer occurs 5-10 km lower, and the intensity is stronger by a factor of 3 or more. It appears likely that the shape of the Na-D emission profile is influenced by the altitude distributions of both sodium and ozone, the reactants that are necessary to produce the emission. The observed variability may be explained by a systematic seasonal mismatch in the altitude of the mesospheric density maxima for sodium and ozone, combined with a known threefold wintertime increase in sodium density.</p> <p><i>hgs:ds</i></p>				
20. DISTRIBUTION/AVAILABILITY OF ABSTRACT			21. ABSTRACT SECURITY CLASSIFICATION	
<input type="checkbox"/> UNCLASSIFIED/UNLIMITED <input checked="" type="checkbox"/> SAME AS RPT. <input type="checkbox"/> DTIC USERS			Unclassified	
22a. NAME OF RESPONSIBLE INDIVIDUAL			22b. TELEPHONE (Include Area Code)	22c. OFFICE SYMBOL

PREFACE

The sodium data were provided by the Aerospace Special Sensor Density instrument team: J. B. Pranke, A. B. Christensen, F. A. Morse, D. R. Hickman, W. T. Chater, C. K. Howey, and D. A. Jones. The author would particularly like to thank A. B. Christensen for his continued support of this research and for many discussions. Conversations with R. R. Meier and G. Sivjee have also been very helpful.

Revision For	
1.1.5 - C2444	↓
1.1.5 - 148	()
1.1.5 - 148	()
By	
Date	
Approved by (Name)	
Unit	Approved by (Name)
A-1	

CONTENTS

PREFACE.....	1
I. INTRODUCTION.....	7
II. INSTRUMENT DESCRIPTION.....	13
III. OBSERVATIONS.....	17
IV. INTERPRETATIONS.....	29
REFERENCES.....	35

FIGURES

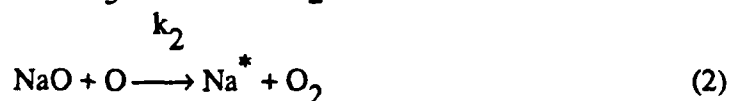
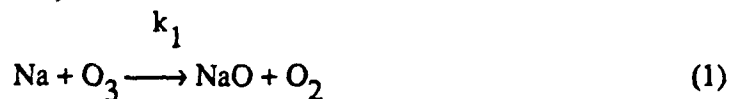
1.	At 2200 Local Evening, the Nighttime Sodium Layer May Have Several Maxima in the Vertical Density Profile.....	10
2.	Atmospheric Ozone Decreases Exponentially Above Its Maximum at 23 km.....	11
3.	Isometric Drawing Showing the Major SSD Systems.....	14
4.	Viewing Geometry for the SSD UV Limb-Scanning Spectrometer.....	15
5.	Typical Data Describing the Count Rate Versus Tangent Point Altitude for a Single Scan of the Limb Are Shown as Squares with Estimated Error Bars on the Count Rate.....	18
6.	When Chapman Fits to Consecutive Limb-Scan Data Are Compared, It Is Apparent That the Tangent Point Altitude, Thickness, and Radiance of the Emission Layer Vary with Latitude.....	20
7.	A Global Distribution of Limb Scans for 1 Day, July 29, 1979.....	21
8.	(a) A Distribution of Limb-Scan Data with Tangent Point Altitude and Latitude for July 29, 1979; (b) A Distribution of Nighttime Na-D Count Rate Versus Tangent Point Altitude and Latitude for a Single Satellite Orbit.....	22
9.	Consecutive Limb Scans from a Nightside Orbit Beginning at 51146 s UT on July 29, 1979.....	24
10.	Same as for Fig. 9, but Beginning at 45786 s UT, July 23, 1979, Showing an Atypical Increase of the Midlatitude Emission in the Summer (Northern) Hemisphere.....	25
11.	A Comparison of the Peak Emission of the Layer Versus Latitude for the Northern Hemisphere for Four Nighttime Passes.....	26
12.	A Comparison of the Tangent Altitude of the Peak Emission for the Four Nighttime Passes of Fig. 11.....	27

FIGURES (continued)

13. The Topside Scale Height of the Line-of-Sight Emission
Increases with Latitude in the Northern Hemisphere..... 28
14. A Demonstration That the Product of the Ozone and
Sodium Densities Would Display the Characteristics
of Our Observed Na-D Peak Emission
Height, Width, and Amplitude..... 30

I. INTRODUCTION

During the night in the earth's upper atmosphere, equilibrium exists between the reactions (Megie and Blamont, 1977)



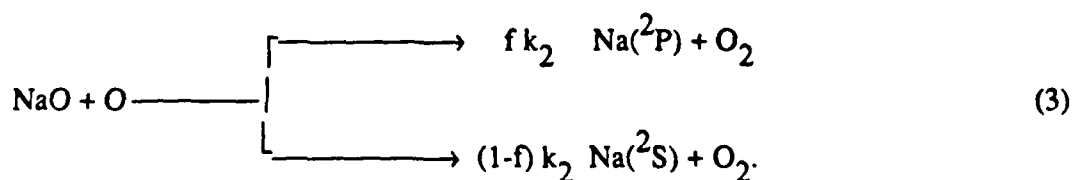
These are the primary production and loss reactions affecting the density of sodium oxide, as well as the major reactions influencing the production of excited sodium. The rate coefficients of the above reactions, taking into account the electron jump mechanism of these bimolecular processes, are given by Kolb and Elgin (1976) as

$$k_1 = 3.3 \times 10^{-10} \text{ cm}^3 \text{ s}^{-1}$$

$$k_2 = 1.6 \times 10^{-10} \text{ cm}^3 \text{ s}^{-1}$$

These reaction rates are still controversial. Recent room temperature experiments by Silver and Kolb (1986) and Ager et al. (1986) have found values of $(3.1 \pm 0.4) \times 10^{-10} \text{ cm}^3 \text{ s}^{-1}$ and $(7.3 \pm 1.4) \times 10^{-10} \text{ cm}^3 \text{ s}^{-1}$, respectively. The reason for this discrepancy is not yet understood. Swider (1986a,b) uses the value $7 \times 10^{-10} \text{ cm}^3 \text{ s}^{-1}$. Whatever value is chosen for k_1 , it is important to recognize that interpretations should be applied only to relative data, i.e., data observed by one instrument during one experiment.

Kolb and Elgin pointed out that the inference of the rates depends on the branching ratio f adopted for reaction (2):



The factor f is the efficiency of reaction (3) in producing excited sodium that emits radiation at 589.0 to 589.6 nm, i.e., the Na-D emission lines. Kolb and Elgin estimated a value of f between 0.01 and 0.1 in order to match observations of nightglow intensities. In part, the uncertainty results from the fact that the Na-D emission varies as the product of the densities of sodium and ozone, both of which display strong variability in the mesosphere (Hunten, 1967; Sipler and Biondi, 1975; Thomas et al., 1984).

The sodium layer has previously been studied both through radiance measurements of the Na-D lines and by lidar instruments from the ground. Lidar measurements of the sodium number densities [Gibson and Sandford, 1971 (51°N); Megie and Blamont, 1977 (44°N); Megie et al., 1978a,b (44°N, 80°N); Simonich et al., 1979 (23°S)] appear to have confirmed previous photometric measurements [Donahue and Blamont, 1961 (23°N); Blamont and Donahue, 1964 (69°N); Hunten et al., 1964 (44°S); Sullivan, 1971 (48°N); Rees et al., 1975 (65°N)] of seasonal variations and latitudinal variations of the sodium total abundance. The lidar measurements examine sodium through resonant scattering from a local region within the layer, while photometers observe a radiance integrated along a line-of-sight passing through the layer. In order for photometric studies to provide estimates of sodium densities, the radiance measurements must be compared to radiances calculated using a theoretical model of sodium emissions.

Researchers from Brazil (Clemesha et al., 1978; Kirchhoff et al., 1981a,b) have compared ground-based lidar observations at 23°S with the intensity of the sodium nightglow to show that local variations in the glow are well correlated with temporal perturbations in the sodium density over periods of 12 h. They observed the nightglow to be best correlated with the sodium density at 88 km, on average 4 km below the maximum sodium concentration. Their data appear to be among the earliest to confirm that the nightglow may be affected by something other than the sodium density alone.

Further long-term, ground-based studies of variations of the sodium layer have been provided by Megie et al. (1978a,b) and by Jegou et al. (1985a,b). They typically observed the height of the peak of the sodium layer to vary by 3 to 5 km and the layer thickness to range from 4 to 14 km. The altitude of the peak sodium density was lower in winter. They also reported a recurrent threefold wintertime increase in the density of sodium above France. Although the long-term sodium behavior was shown to be only weakly sensitive to vertical winds or steady electrostatic fields, these effects were shown to help establish the trend toward a lower altitude of the sodium layer in winter.

While these general features persist, it is difficult to predict the sodium layer shape at a particular location and time. Researchers agree that the total content of the sodium layer is very steady, having an evolution time constant of greater than 3×10^4 s. The shape of the sodium layer, however, is strongly influenced by dynamical processes such as random occurrences of eddy mixing (Megie and Blamont, 1977) or gravity waves (Shelton and Gardner, 1981), or tides (Batista et al., 1985). Figure 1 illustrates a typical perturbed shape of the sodium layer [based on a 2200 local time (LT) plot within Fig. 9 of Gardner et al., 1986a], demonstrating the difficulty in defining the layer height and thickness as the layer varies from a broad square shape to a narrow peaked structure. While describing diurnal variations in vertical perturbations of the layer above Illinois, Gardner et al. introduced the concept of a centroid height to define a mean altitude for the layer, usually occurring between 90 and 93 km.

Similarly thorough studies have shown that mesospheric ozone also tends to be sensitive to dynamical processes. Ground-based measurements of Evans et al. (1968) and others have characterized the mesospheric vertical profile for ozone. Atmospheric ozone is seen to be a thin layer near 23 km, decreasing exponentially up to the mesosphere, where it usually displays a minor, variable secondary maximum near 80 to 90 km, as represented in Fig. 2.

The total ozone content integrated vertically through the atmosphere has been monitored for years from a network of ground-based stations distributed globally. A seasonal maximum of total ozone occurs at high latitude (60-70°) during local spring, as described by Dobson (1968) and London (1980). Thomas et al. (1983, 1984) deduced ozone densities from 1.27 μ m airglow measured from the Solar Mesosphere Explorer Satellite. They showed the seasonal variability of ozone at 80 km to be semiannual, with a stronger maximum in the spring than in the autumn. The spring maximum may reach a factor of 1.6 to 3 greater than the minimum value. This suggests that the seasonal dependence of mesospheric ozone is not likely due to chemistry alone. Photochemistry would promote an inverse relationship between the ozone density and atmospheric temperature, which would imply a maximum ozone density in summer, when the mesopause temperature is coldest at middle and high latitudes (Solomon et al., 1983; Thomas et al., 1984). Although the ozone density in the mesosphere varies rapidly at dawn and dusk, it is relatively constant during the night, except within a few kilometers of the mesospheric density maximum (Kirchhoff and Clemesha, 1983). Work by Kirchhoff

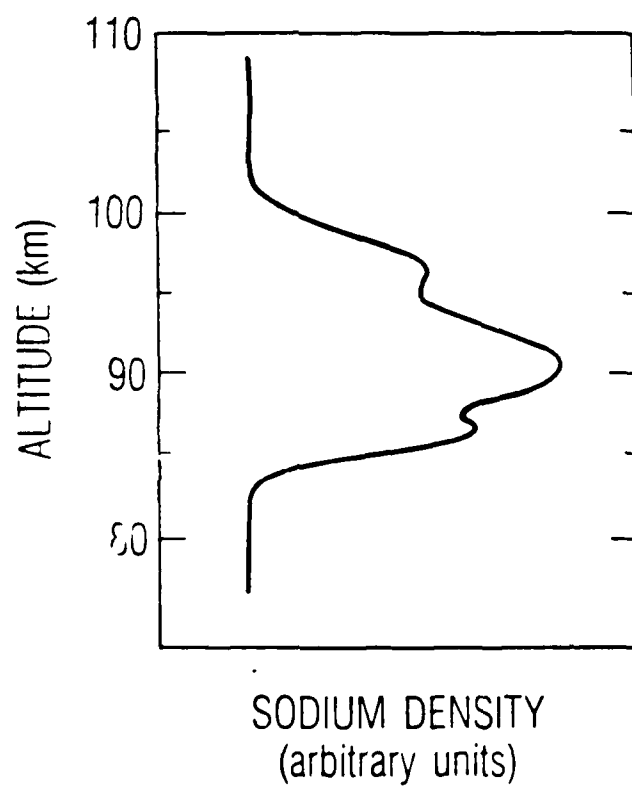


Fig. 1. At 2200 Local Evening, the Nighttime Sodium Layer May Have Several Maxima in the Vertical Density Profile. A nighttime peak sodium density of $5 \times 10^3 \text{ cm}^{-3}$ is typical.

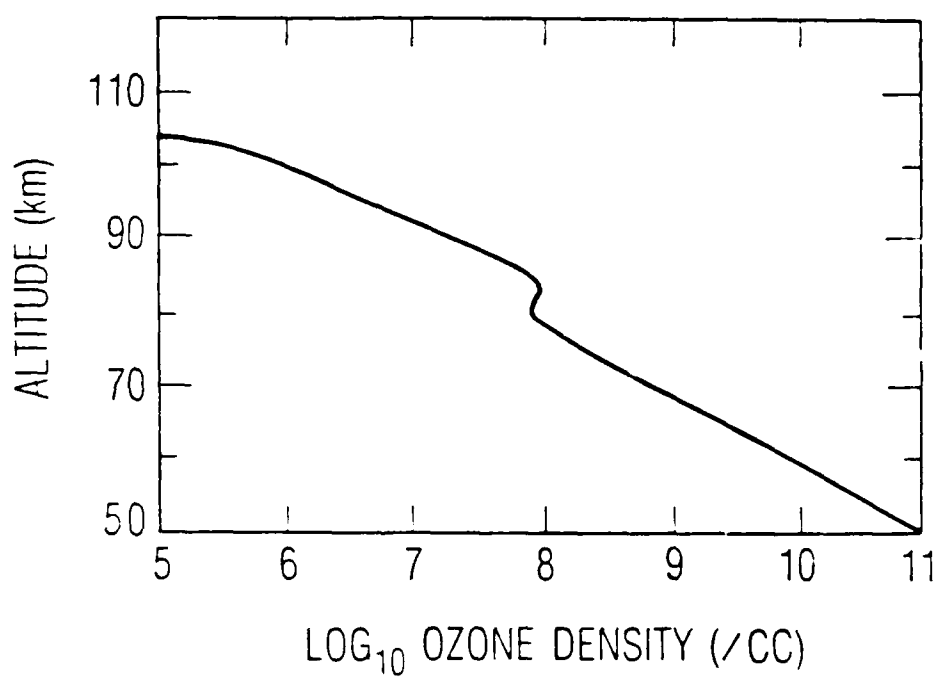


Fig. 2. Atmospheric Ozone Decreases Exponentially Above Its Maximum at 23 km. Near 80 km, chemistry and dynamics cause a local redistribution of ozone.

et al. (1981a) was the first to suggest a connection between observed rapid variations in the Na-D emissions with height near the maximum at 80 km, and known diurnal variations of the ozone density.

Also, very recently, Swider (1986a) made a connection between the known equinoctal maxima of ozone and a less well known peak in the sodium nightglow at the equinoxes [Smith and Steiger, 1968; Kirchhoff et al., 1979]. He suggested that in the chemistry of the sodium D-line nightglow the sodium remained unconsumed, and that the seasonal variations of sodium density and the nightglow were uncoupled.

In this report, the correlation of sodium nightglow with sodium and ozone densities has been pursued further. The variability of limb-scan nightglow emissions has been investigated globally and compared with known mesospheric sodium and ozone density variations. Photometric observations near 589.0 nm from a 1979 satellite flight were analyzed to determine the global variability of the nighttime mesospheric sodium-doublet emission. Our data correspond to a local time of about 2200 LT. Although we recognize that there are often two or three distinct sodium layer maxima [Gardner, 1986b], our limb-scan data tend to smooth out any effect of layering.

Since the density of sodium is greater during local winter, it was expected that maximum intensities for the Na-D emissions would be obtained in the Southern hemisphere for our data, obtained in late July. Seasonal differences in the amplitudes of Na-D emissions observed by the instrument in the northern and southern hemispheres were indeed confirmed; however, observed systematic variations in the layer shape could not be explained by the known variability of atmospheric sodium densities or of ozone alone. We will show that the thickness and shape of the emission layer appear to be explained by a mismatch in the altitudes of density maxima of the sodium and ozone layers.

II. INSTRUMENT DESCRIPTION

Observations of the atmospheric sodium doublet at 589.0 to 589.6 nm were obtained from a photometer included as part of the limb-scanning ultraviolet spectrometer, designated SSD, flown on a Defense Meteorological Satellite Program satellite (DMSP-F4). The spectrometer consisted of a 0.5 m concave grating in a Wadsworth mount, a mechanical modulation collimator to define the field of view, and multiple exit slits and detectors. A drawing of the instrument is shown in Fig. 3. A more complete description of the experiment is provided by Pranke et al. (1982).

The atmospheric sodium emission was detected by allowing the undiffracted central image beam in the spectrometer to be reflected from a dichroic mirror and to pass through a narrow bandpass interference filter to a photomultiplier tube, operated in a photon-counting configuration. The interference filter was centered at 589.0 nm, with a bandpass of 5.7 nm and a peak transmittance of 78%. The field of view was $0.14 \times 3.75^\circ$ [full width at half maximum (FWHM)], corresponding to an altitude span of approximately 6 km at the tangent point. The effective aperture was 4 cm^2 . For the data in this report, the instrument was operating in a limb-scanning mode where the instrument stepped through its complete range of 40 elevation angles, from -26.54 to 18.16° , corresponding to tangent point altitudes from approximately 70 to 470 km on the limb (see Fig. 4). Counts were accumulated in the Na-D channel for a dwell period of 1 s. A limb scan required 4 s at each of 40 positions, plus 4 s to return to the initial scan position--a total period of 164 s for each scan cycle. The profile measurements are separated by approximately 10° in latitude. The motion of the satellite was compensated by the limb scan, so that the tangent point location moved only 3° in latitude during each vertical scan and 7° between scans.

The responsivity of the Na-D photometer channel was determined viewing a diffuse reflective screen illuminated with a calibrated tungsten iodide light source. The output signal was measured versus grating angle. The responsivity peaked at a value of 4.8×10^{-2} counts $\text{Rayleigh}^{-1} \text{ s}^{-1}$ (cts $\text{R}^{-1} \text{ s}^{-1}$). For the flight data, counts have been weighted and summed for each of the four wavelength positions. The resultant effective responsivity of the Na-D channel was $0.13 \text{ cts R}^{-1} \text{ s}^{-1}$.

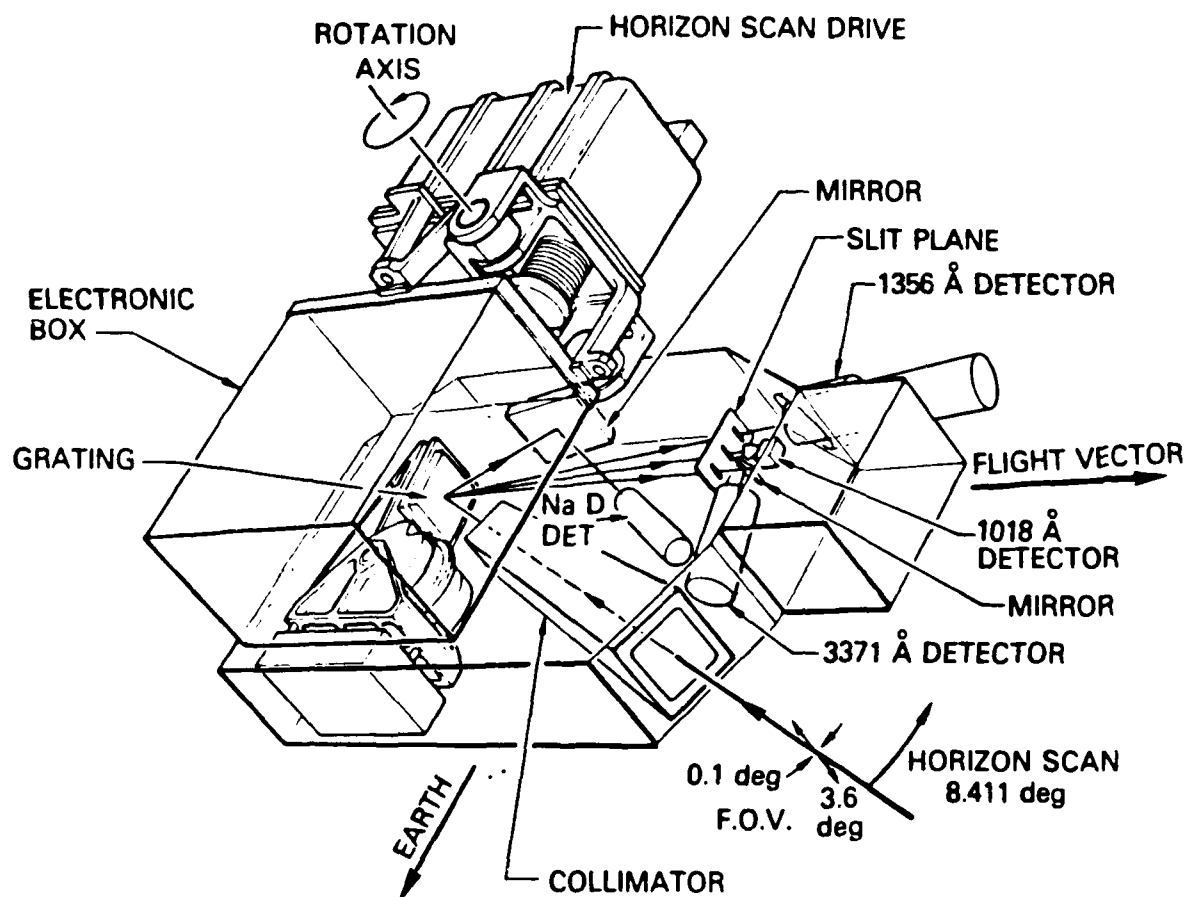


Fig. 3. Isometric Drawing Showing the Major SSD Systems. The limb-scan drive and electronics box were mounted to the spacecraft. The optics box was mounted to a shaft through the limb-scan drive. The modulation collimator defined the field of view ($0.14 \times 3.5^\circ$). Light diffracted in the first order was focused on the near ultraviolet (UV) detector, second order on the far ultraviolet (FUV) detector, and third order on the extreme ultraviolet (EUV) detector. The undiffracted central image was directed to the dichroic mirror and onto the NaD detector.

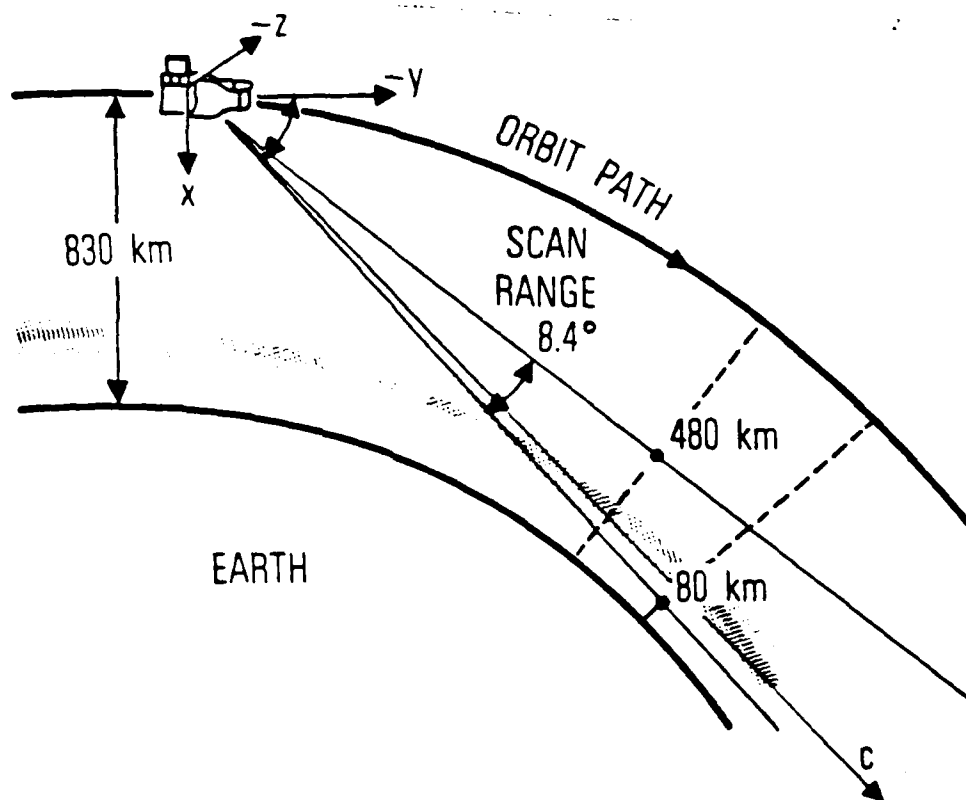


Fig. 4. Viewing Geometry for the SSD UV Limb-Scanning Spectrometer. The satellite traversed a circular, 830 km altitude, sun-synchronous orbit with an inclination of 98.8°. It was three-axis stabilized with the x-axis perpendicular to the local reference ellipsoid. The angle scan nominally covered tangent heights from 70 to 470 km.

III. OBSERVATIONS

The SSD instrument was launched on 6 June 1979 into a near circular sun-synchronous orbit with a northbound equatorial crossing maintained at 2200 LT at an altitude of 830 km. The instrument continually scanned across the earth limb ahead of the satellite along the satellite track. Observations of the atmospheric sodium emission in the appropriate instrument mode were obtained on 23 July [day 204 universal time (UT)] and 29 July (day 210 UT) 1979. These observations occurred on the nightside of the earth when the spacecraft was in the earth's shadow.

Data for a single limb scan (e.g., Fig. 5) displayed a peak in the sodium nightglow intensity as the line of sight of the instrument crossed the mesospheric sodium layer. Recall that each data point represented the integrated emission along a line of sight. The local sodium D-line emission was proportional to the product of sodium and ozone densities, assuming reactions (1) and (2) to be in equilibrium. Each profile of emissions, such as that shown by squares in Fig. 5, was plotted versus tangent point altitude, i.e., the height of the closest approach to the earth of the line of sight across the earth's limb.

Our observed maximum limb intensities were a factor of 60 greater than the average values of 40 to 60 R seen in the zenith nightglow by Kirchhoff et al. (1979, Fig. 4) from the ground. This agrees with comparisons of the ratio of limb-to-nadir integrated emissions estimated using the Chapman grazing incidence function and calculated by integrating a model emission along the limb and nadir lines of sight. The data (e.g., Fig. 5) have been fit with a Chapman function for convenience, using the formulation

$$I = I_0 \exp \{ 1 - (z - z_p)/H - \exp[(z_p - z)/H] \} \quad (4)$$

to estimate the altitude of the peak, z_p , and the topside scale height, H . No small-scale structure is expected to be observable in the emission profile due to the smoothing effect of integrating the radiance through the layer along the line of sight. By performing an integration over the instrument line of sight, one can show that the curvature of the atmosphere provides a maximum integrated emission when the tangent point of the line of sight of the instrument is below the altitude of peak emission by about a kilometer. The

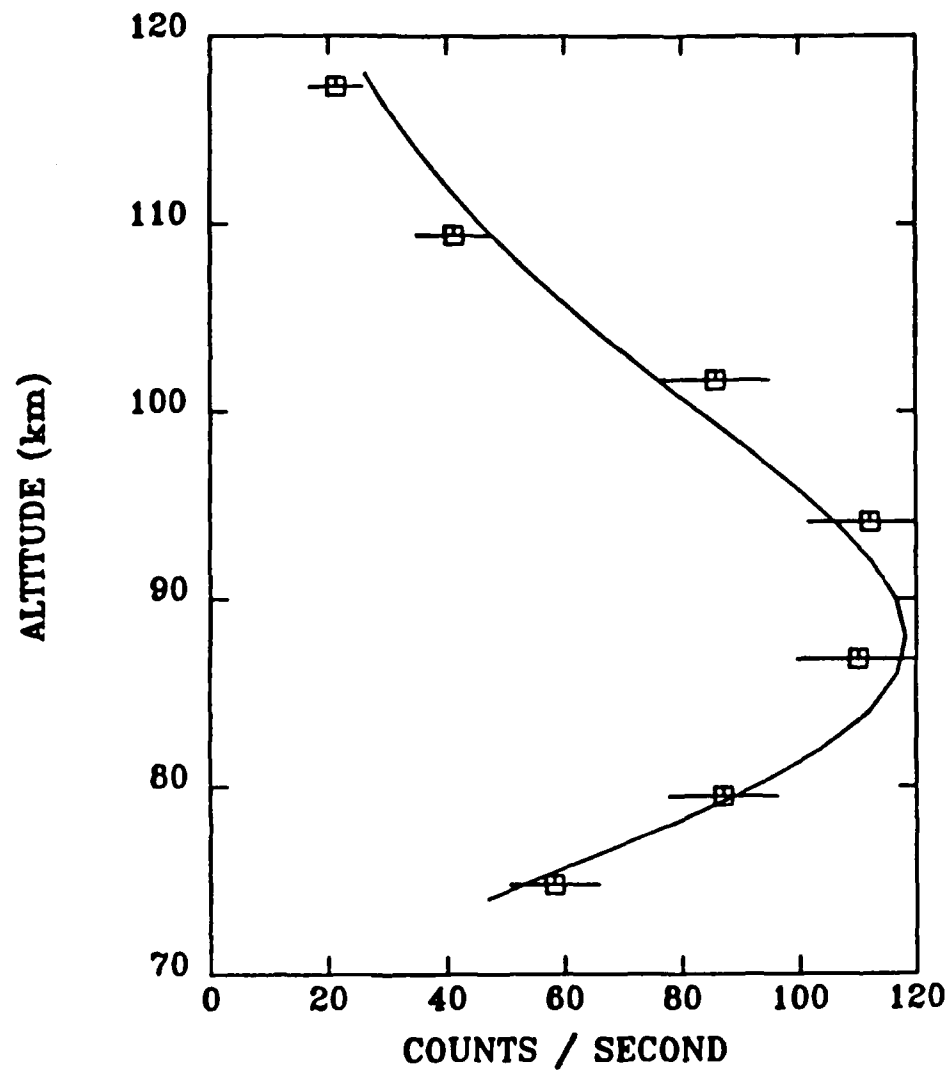


Fig. 5. Typical Data Describing the Count Rate Versus Tangent Point Altitude for a Single Scan of the Limb Are Shown as Squares with Estimated Error Bars on the Count Rate. The data, in this case taken on July 23, 1979, at 38°N latitude and 101°E longitude, have been fit by a Chapman function to determine the tangent altitude of the peak emission.

width of the emission profile at half the maximum intensity is $0.53 (\pm 0.01)$ times the width of the observed limb-scan profile.

When Chapman function fits to limb-scan data from a single nightside orbit are plotted together for a variety of latitudes, as in Fig. 6, it is clear that the shape of the emission layer varies strongly with latitude. Information about the height of the peak emission is lost for observations in the southern hemisphere, where the instrument did not scan the limb at or below the peak of the emission layer. For the limb scans that did detect a peak, the thickness of the layer is greater, and the height of the peak is higher, in the summer hemisphere at midlatitudes. Near the equator and in the winter hemisphere, the topside scale height is noticeably smaller. Near the equator, the emissions are a factor of 3 stronger than for northern midlatitudes, and the altitude of the peak is lower. For purposes of comparison, the estimated topside scale height at 42°N latitude is 10.3 km, while it is 6.8 km at 3.4°N ; the height of the peak emission is 93 km at 42°N but only 77 km at 3.4°N . The peak intensity is a factor of 2.8 higher at the lower latitude.

These single scans are representative of data taken during a series of orbits of the instrument on July 23 and 29, 1979. Figure 7 illustrates typical global data coverage for 1 day. Each cross represents the tangent point location in latitude and longitude where a good altitude scan of the sodium layer was obtained. Data obtained while the instrument was looking into the sunlit hemisphere or while passing over the South Atlantic Anomaly were contaminated by scattered sunlight and energetic particles, respectively, and were discarded.

The altitude dependence of individual scans over 1 day is shown in Fig. 8a. All altitudes were calculated from satellite ephemeris information, assuming that the earth's surface could be represented as a geoid with major axis 6378 km and minor axis 6357 km. Since the satellite perigee was on the dayside of the earth, the minimum altitude of these nighttime observations obtained near 15°N latitude was not indicative of instrument perigee. It is assumed that the variability in the altitude scan range was due to both a lack of circularity of the orbit and due to altitude variations in the earth's surface with respect to the geoid. Since the instrument did not scan below the peak of the emission layer in the southern hemisphere, it is more difficult to contrast summer and winter hemisphere measurements. Nevertheless, strong trends occur in the data, as evidenced in plots of instrument count rate versus latitude and altitude, such as displayed in Fig. 8b. Latitudinal variations of the count rate indicate an increase by factors of at least 3 as the observations

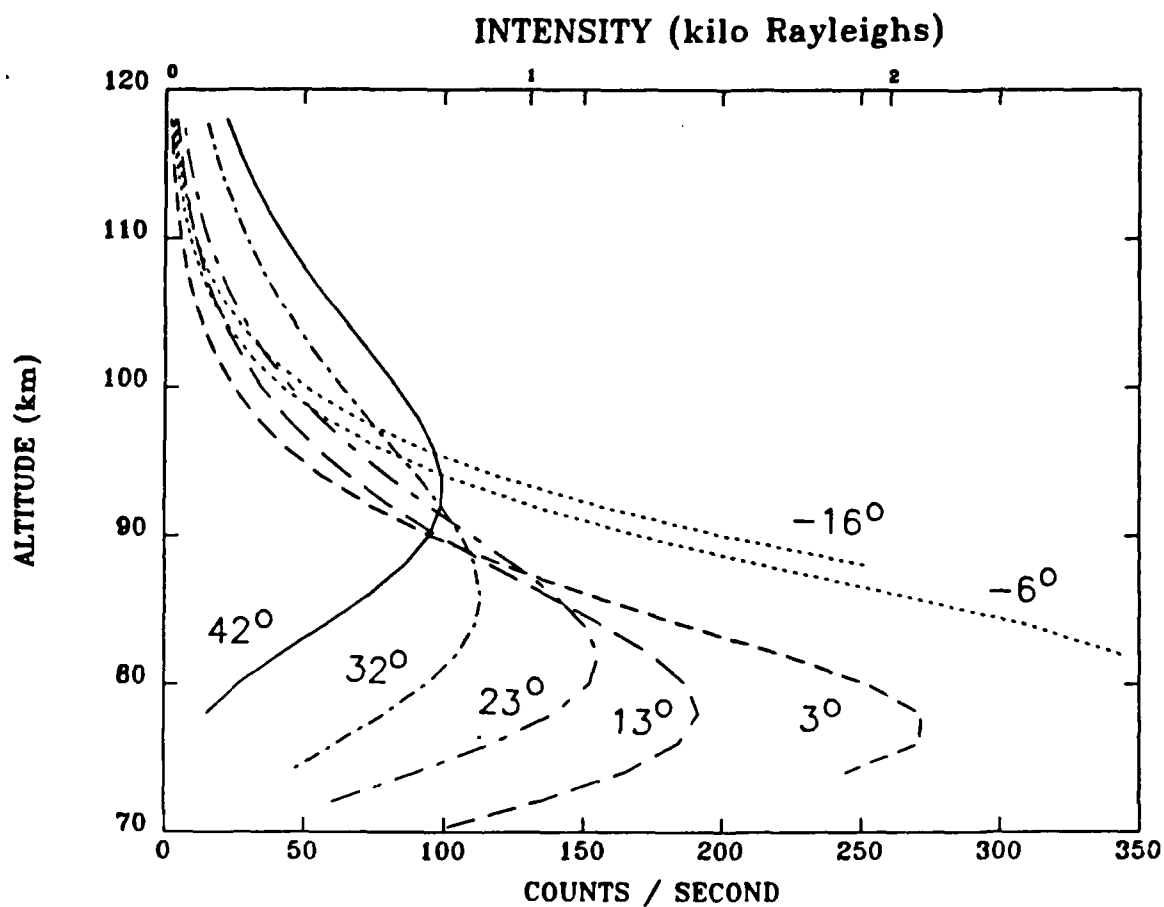


Fig. 6. When Chapman Fits to Consecutive Limb-Scan Data Are Compared, It Is Apparent That the Tangent Point Altitude, Thickness, and Radiance of the Emission Layer Vary with Latitude. The nightglow data were from a single orbit on July 23, 1979.

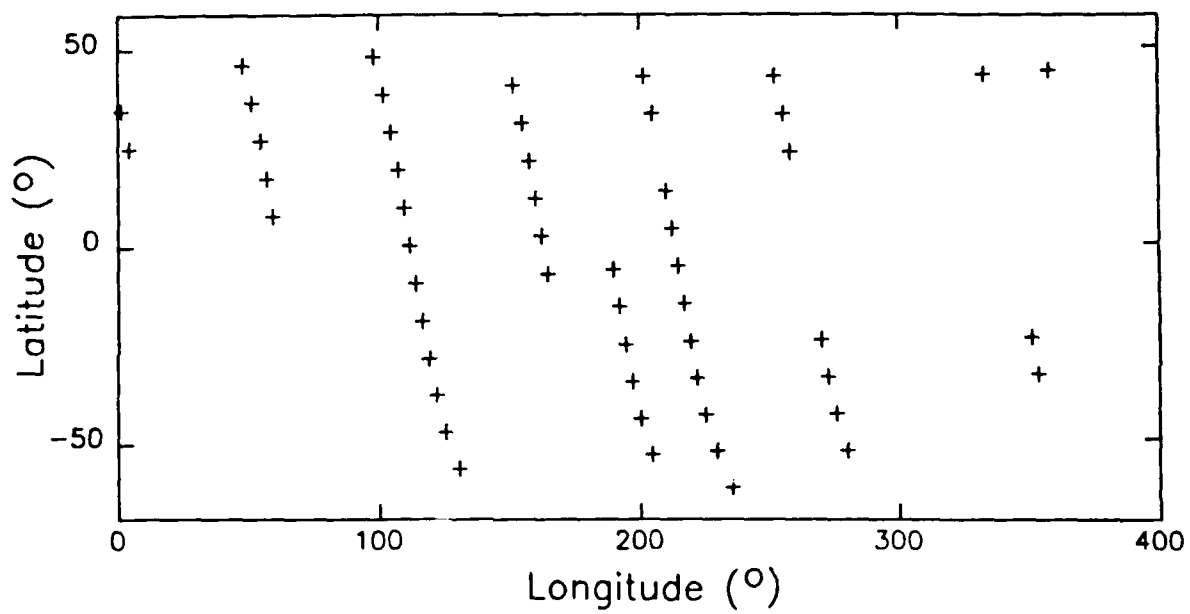


Fig. 7. A Global Distribution of Limb Scans for 1 Day, July 29, 1979

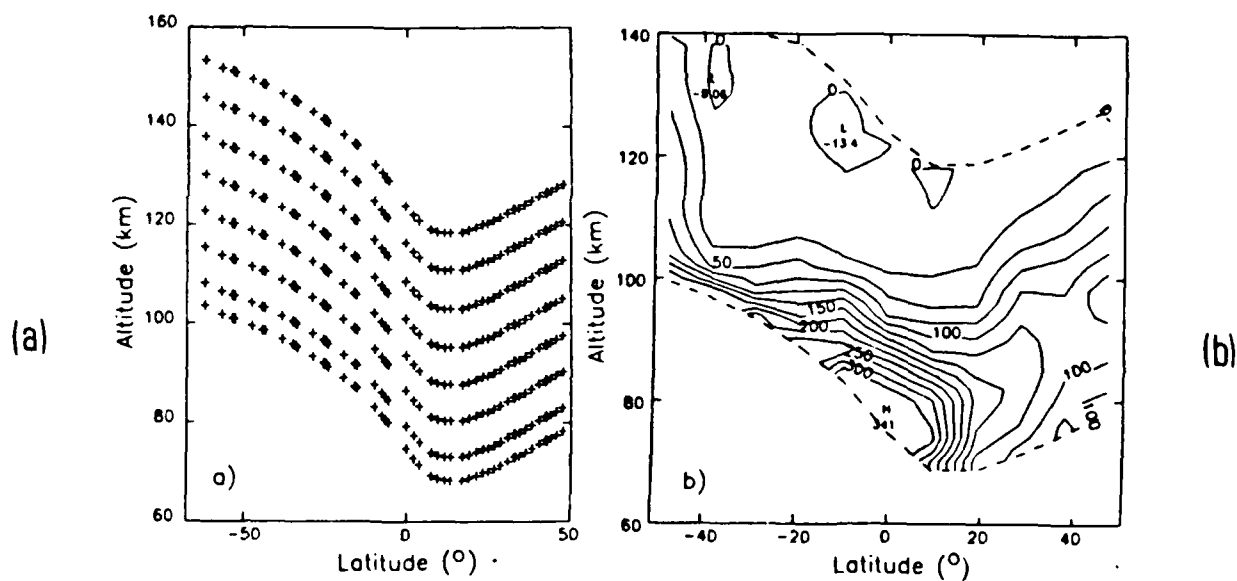
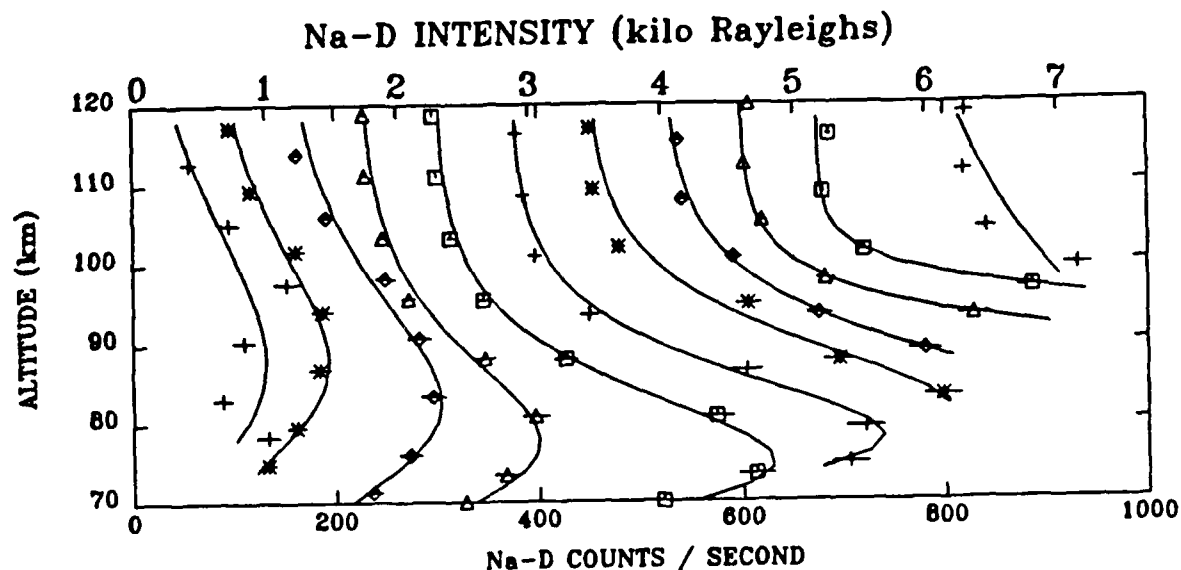


Fig. 8. (a) A Distribution of Limb-Scan Data with Tangent Point Altitude and Latitude for July 29, 1979; (b) A Distribution of Nighttime Na-D Count Rate Versus Tangent Point Altitude and Latitude for a Single Satellite Orbit. Southern hemisphere limb scans did not view below the peak in the emission layer.

pass from the northern to the southern hemisphere. Figures 9-10 show that the character of the latitudinal variation is reproducible over many orbits and indeed over a span of several days. No longitudinal variability is observed.

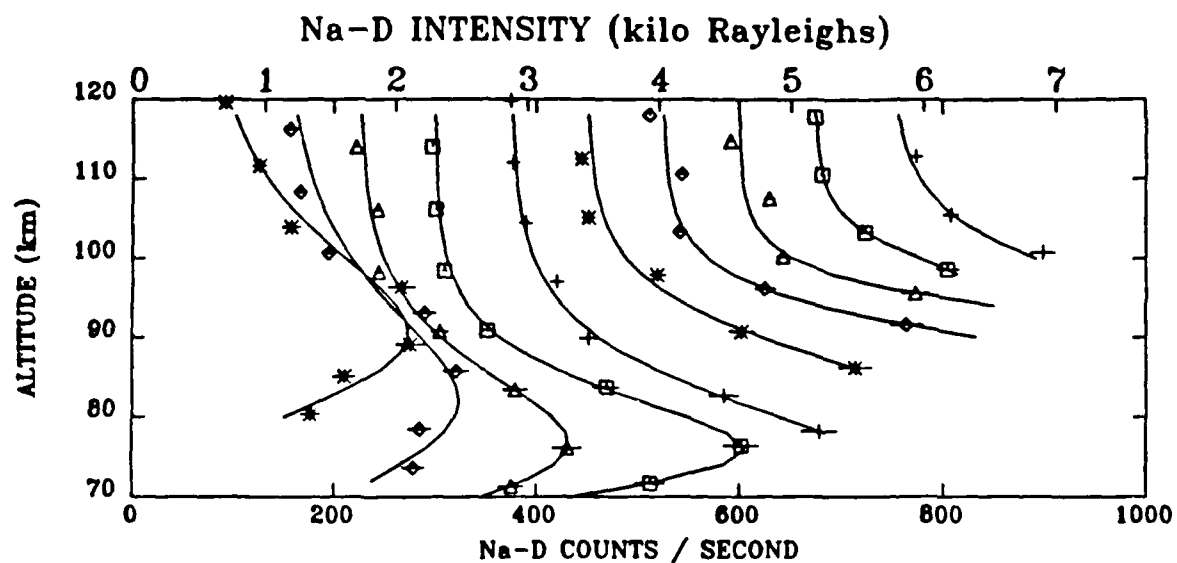
Figures 9-10 illustrate well the general smooth shape that is expected from line-of-sight observations. It is also clear that the Chapman function fit to the profile shape becomes less satisfactory at higher latitudes in the northern hemisphere where the emission appears weaker and the data can be somewhat irregular. Near the equator, the estimated scale height of the emission layer approaches the altitude resolution of the instrument of 6 km. The Chapman height of the peak emission could then be in error by as much as 3 km. For southern hemisphere data, the instrument did not scan below the peak of the emission layers, so the Chapman fits simply serve to aid the eye in following trends in the data. For these scans, the fitted estimates of the peak emission, altitude, and scale height for southern hemisphere scans cannot be relied upon and are useful only in emphasizing the sharpness of the decrease in intensity on the topside. Overall trends in the northern hemisphere data are investigated in Figs. 11-13 for four typical nighttime passes. Although the peak limb-scan intensity displayed in Fig. 11 may vary by as much as 50% from one orbit to the next, it is always the case that the intensity observed at the peak of the layer is lower in the midlatitude summer hemisphere and is higher near the equator. It is not confirmed that the winter hemisphere peak intensities are higher since the instrument generally did not scan below the peak for these data sets. The data, however, do suggest this trend.

The latitudinal dependence of the tangent height of the peak emission is described in Fig. 12 for the same four orbits. It is clear that the tangent point altitude of the peak decreases smoothly from near 90 km in the northern midlatitudes to below 80 km in the equatorial region. At the same time, the topside scale height shown in Fig. 13 also decreases significantly from northern midlatitudes to the equatorial region. These clear trends suggest possible explanations for the variability of the altitude of the peak intensity observed by the SSD instrument.



Lat	48	38	29	19	10	0	-10	-19	-29	-38	-47
Long	98	102	105	107	110	112	114	117	119	122	126
SZA	103	112	120	128	136	143	148	152	153	150	146
I (kR)	1.0	0.9	1.2	1.4	2.5	2.8	2.7	4.1	9.7	3.8	7.2
Z _p	88	88	83	78	75	78	81	78	82	92	42
H	16	12	12	9	8	7	7	7	4	3	21

Fig. 9. Consecutive Limb-scans from a Nightside Orbit Beginning at 51146 s UT on July 29, 1979. The origin of each scan has been displaced 75 counts from the previous scan to facilitate comparisons. The latitude, longitude, and solar zenith angle (SZA) of the tangent point of the limb scan have been tabulated along with the peak Na-D intensity of the layer, I, the tangent altitude of the peak emission, z_p , and the topside scale height, H, of the Chapman fit to the line-of-sight emission layer. The latter fitting parameters are not meaningful for southern hemisphere data, which do not identify a tangent altitude of peak emission.



Lat	38	28	18	9	-1	-10	-20	-29	-39	-48
Long	124	127	130	132	134	137	139	142	145	148
SZA	112	120	128	136	143	149	152	153	151	146
I (kR)	1.5	1.3	1.6	2.3	2.8	2.4	3.5	4.1	1.2	2.3
Zp	91	82	77	76	74	82	85	89	96	92
H	9	10	8	6	7	6	4	3	3	5

Fig. 10. Same as for Fig. 9, but Beginning at 45786 s UT, July 23, 1979, Showing an Atypical Increase of the Midlatitude Emission in the Summer (Northern) Hemisphere

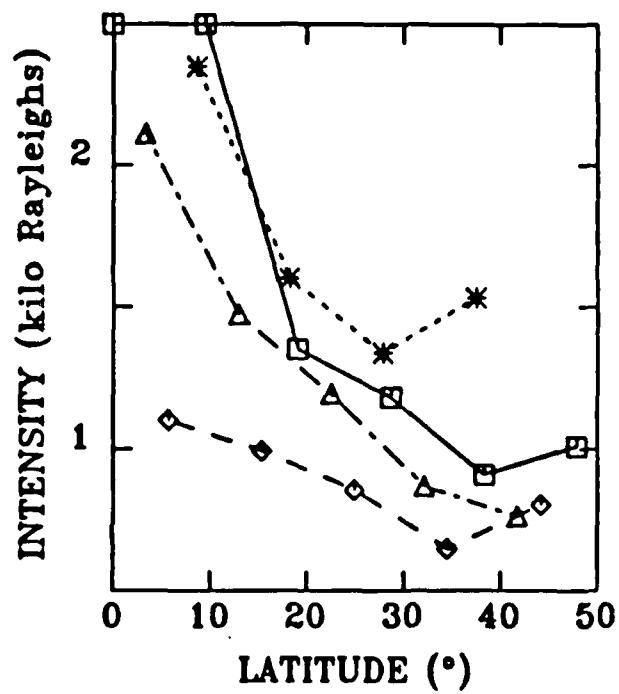


Fig. 11. A Comparison of the Peak Emission of the Layer Versus Latitude for the Northern Hemisphere for Four Nighttime Passes. The intensity is consistently higher near the equator than at midlatitudes.

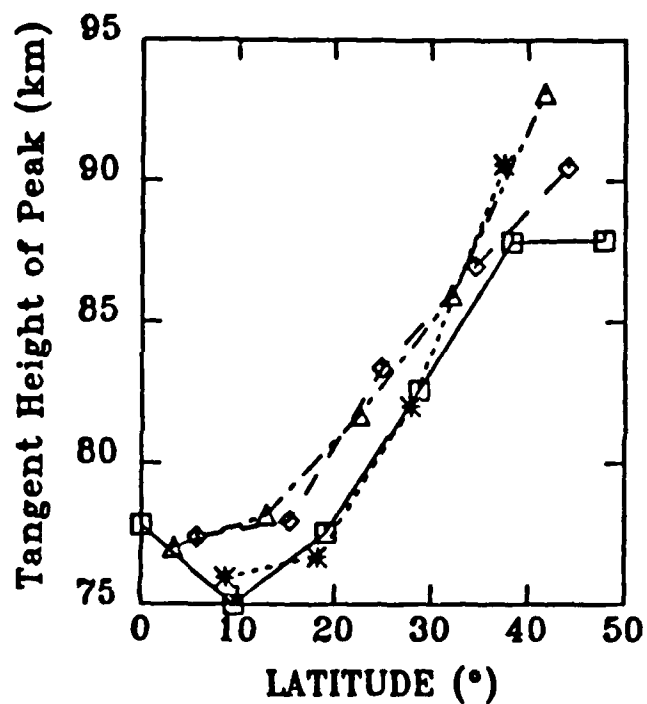


Fig. 12. A Comparison of the Tangent Altitude of the Peak Emission for the Four Nighttime Passes of Fig. 11. The tangent height appears to be relatively constant at a minimum value for latitudes in the range $0 - 20^\circ (\pm 2^\circ)$ and linearly increases with latitude in the range $20-40^\circ (\pm 2^\circ)$.

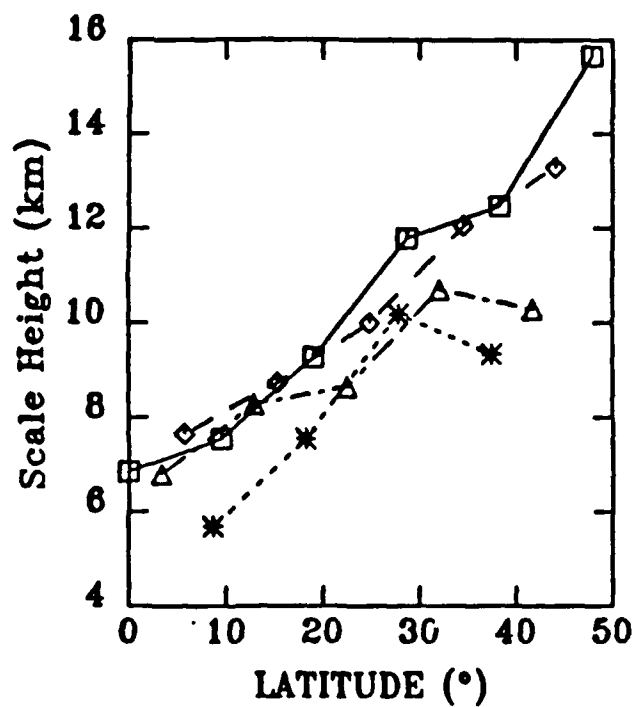


Fig. 13. The Topside Scale Height of the Line-of-Sight Emission Increases with Latitude in the Northern Hemisphere. These data describe the same four nightside passes as Fig. 11.

IV. INTERPRETATIONS

In past studies, it has usually been assumed that Na-D emissions provided a direct reflection of the character of the mesospheric sodium layer (most recently: Clemesha et al., 1978; Kirchhoff et al., 1981a,b) or of the ozone layer (Swider, 1986a). This controversy over establishing which constituent could determine the character of the nightglow emissions has been precipitated by a lack of predictability due to the dynamic variability of the layers. Individual observations of sodium density profiles show considerable variability, sometimes masking the hourly, daily, and seasonal behavior. Occasionally, sodium layers more than 15 km thick have been seen before midnight, extending to altitudes as low as 80 km (see measurements taken above Massachusetts; Gardner et al., 1986b). Similarly, systematic latitudinal variations of the altitude profile of the ozone density are within the range of variability commonly interpreted as due to gravity waves or other dynamical processes. The advantage of our data set is the consistency and repeatability of these global observations, allowing the detection of steady trends. The reproducible latitudinal trends in the thickness and the height of the emission peaks in our data suggest that the altitude variations of both sodium and ozone densities determine the character of the sodium nightglow profile near the mesospheric ozone peak.

Since it is the product of these densities that determines the Na-D line emission, the shape of the emission layer may or may not match well the shape of the sodium density profile. In the summer hemisphere, both sodium and ozone layers are at somewhat higher altitudes than in winter (Jegou et al., 1985b; Thomas et al., 1983; Barth et al., 1983). If the summer mesospheric ozone peak was of minimal amplitude (as suggested by Thomas et al., 1983) or occurred 10 km lower than the sodium peak, the Na-D emission could be relatively broad and centered near the expected centroid of the sodium layer at about 90 km. Our summer hemisphere observations would then follow directly. This is illustrated in Fig. 14a, where the sodium density is multiplied by the ozone density to model a broad Na-D emission layer, labeled P.

In the winter hemisphere, the peak sodium density is known to increase by a factor of 3 or more over the seasonal minimum, and the altitude of the peak density is known to be lower by 3 to 5 km (Jegou et al., 1985a,b). Figure 14b illustrates a Na-D emission

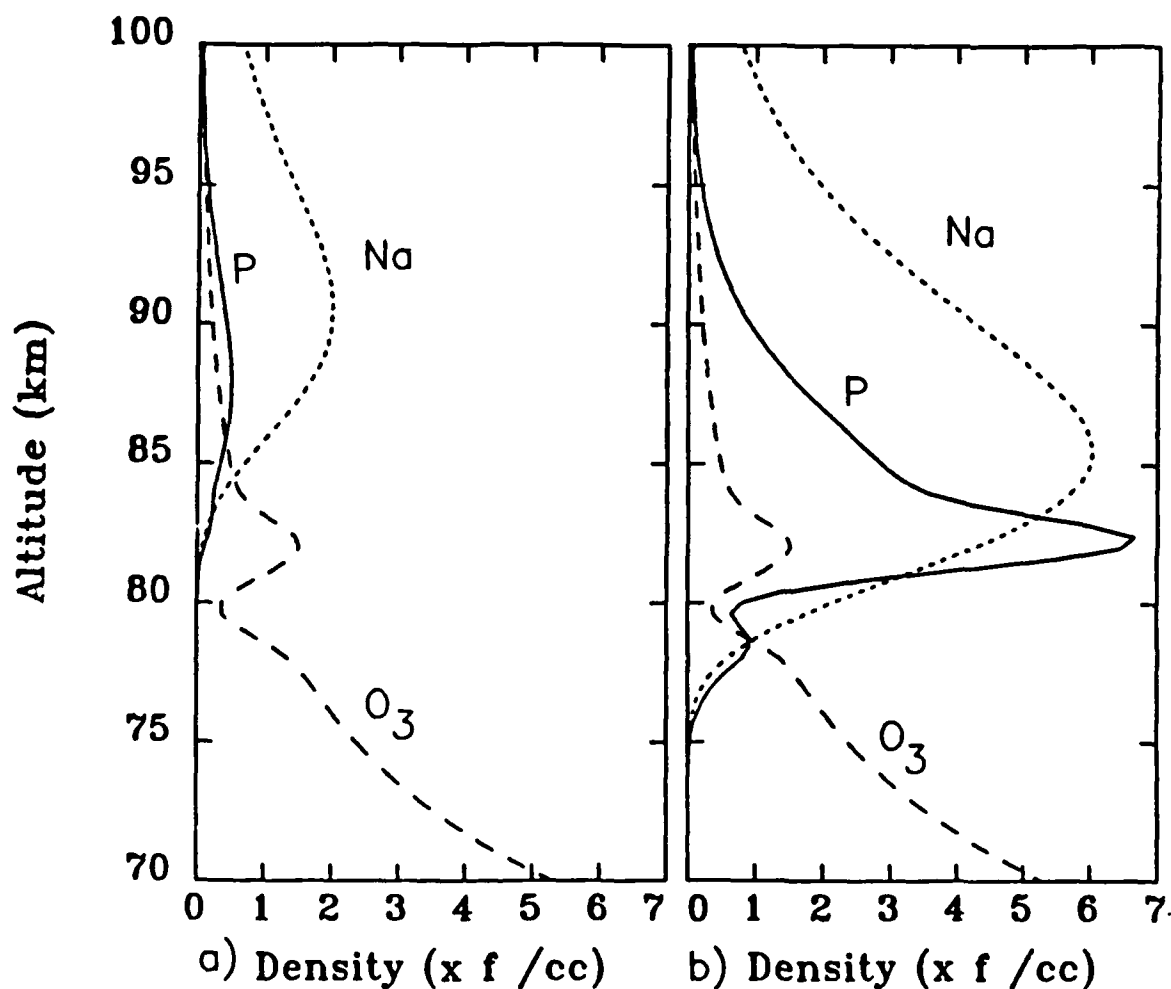


Fig. 14. A Demonstration That the Product of the Ozone and Sodium Densities Would Display the Characteristics of Our Observed Na-D Peak Emission Height, Width and Amplitude. (a) Summertime sodium density ($f = 10^3$), ozone density ($f = 10^8$), and product of sodium and ozone densities, $P(f = 10^{11})$. The sodium has been modeled by a Chapman function with upper and lower scale heights of 5 and 4.5 km, respectively. The ozone density is represented by an exponentially decreasing function of altitude perturbed by a Maxwellian cavity at 79.8 km and a symmetrical Maxwellian enhancement (containing the same amount of ozone) at 82.2 km. (b) Wintertime density profile displays a low altitude narrow peak, assuming only a typical winter increase by a factor of 3 in the sodium density and known 3 km lowering of altitude of the sodium peak density.

layer that would result if one assumed only these changes in the sodium layer of Fig. 14a. A sodium layer was centered near 87 km, and a mesospheric ozone peak was again assumed near 82 km altitude. The resulting profile for Na-D is very sharp and displays a maximum near 82 km, well below the maximum density of the sodium layer. The factor of 3 or more change in the Na-D emission is directly due to a proportional increase in the sodium density. The narrow profile is very similar to the equatorial limb scans of Figs. 9 and 10. One difference is that the strong maxima observed near 3.4°N have tangent altitudes as low as 77 km. This is somewhat deceptive, because the tangent height of the peak line-of-sight emissions must appear somewhat lower in altitude than the actual peak of the emission layer. The curvature of the emission layer over 1000 km of the line of sight makes a limb-scan layer maximum appear lower than the altitude of maximum emission by 1 km or so, depending on the layer shape. Since our data have an altitude resolution of 6 km, the Chapman fit introduces a further uncertainty of 3 km in the altitude of the peak emission. We assume that with better altitude resolution, the peak emission layer near 3.4°N would be identified near or above 80 km.

Figure 14 illustrates that sharp Na-D profiles are reasonable if one takes into account known seasonal variations in the altitude and density of sodium. Variations in the product of sodium and ozone also explain the differences between the observed Na-D profiles and the characteristic variability of sodium. The centroid height of the sodium layer varies from 90 km by at most 3 to 5 km, and the sodium layer thickness in late summer is known to vary from 4 to 14 km (Jegou et al., 1985a,b). Our Na-D data reveal systematic latitudinal variations in both the layer thickness and altitude, which are likely due to a seasonal separation of the sodium and ozone maxima. While Megie and Blamont observe the sodium topside scale height to decrease with an increase in the altitude of peak density, our data display the opposite tendency, because the scale height of Na-D emissions is broader in the summer hemisphere, where the maxima of the two constituents are separated by about 10 km.

A number of possible ozone and sodium density models have been utilized to simulate such sodium-D emission layers. The two examples of Fig. 14 were able to account for the observed Na-D emission without requiring any variability in the ozone profile. Once the ozone variability is taken into account, the sodium nightglow emissions are even more difficult to predict. Consider the low latitude study of mesospheric ozone by Hays and Roble (1973). Often their data showed sharply reduced ozone density in the 10 km region immediately below the peak of the mesospheric layer. This kind of behavior

was also suggested by other published nighttime ozone altitude profiles, such as those given in Fig. 3 of Green et al. (1986). In one of our examples, we observed that if such a reduction in the ozone density occurred just below the peak of the sodium density, then the sodium-D emission layer could split into two sharp layers. Depending on the mismatch of sodium and ozone, one of the resulting emission layers could be an order of magnitude less intense than the other and would contribute only minimally to instrument limb scans of the region. This would also result in the detection of a very thin layer similar to the layers shown in Figs. 9-10 for latitudes near the equator. We conclude that sharp ozone density depletions could also, on occasion, produce thin Na-D emission layers at low altitudes, but such layers may be produced in simpler ways. One further possibility is suggested by the models of Hingane (1984), which predict a double peak for ozone with maximum densities near 75 and 85 km. Most data suggest a single ozone peak (if any) between 80 and 95 km; however, the interaction of a sodium layer mismatched in altitude with such dual ozone layers could also produce thin Na-D emission layers.

In summary, the shape and altitude of both the mesospheric ozone and the mesospheric sodium density maxima strongly influence the shape of the Na-D emission profile. It is suggested that in the summer hemisphere, the density maxima of sodium and ozone are separated in altitude. This could explain the smooth, broad Na-D emission profiles seen in these regions. In the winter hemisphere, the peak sodium density is known to be greater by a factor of 3 than the summer hemisphere peak density (in the midlatitude study of Jegou et al., 1985b), hence increasing the Na-D emissions proportionately. Sharper Na-D profiles are seen during winter, when the sodium and ozone maxima are likely to be more closely aligned. These features may explain our equatorial scans and suggest the character of Na-D emissions in the southern hemisphere data as well. Further discussion must await detailed modeling of the Na-D emissions with latitudinally dependent sodium and ozone vertical density profiles.

We have not yet mentioned possible solar cycle effects. Our data were obtained during solar maximum conditions and should compare better with the solar maximum lidar observations of Gibson and Sandford (1971) than to the near solar minimum lidar results of Jegou et al. (1985b). The former authors presented seasonal variations of a factor of 10 in sodium column density and a strong seasonal variation of 8 km in the height of the sodium peak density. Their wintertime sodium peak densities were centered quite low, ranging from 87 to 89 km altitude. The February 1/August 1 ratio of sodium column number densities was a factor of 3. These data correspond reasonably well to our

photometric observations. Gibson and Sandford observed the altitude of the sodium peak to be higher in early February than in early August. Nevertheless, a more pronounced profile mismatch would have existed in summer, because the width of the sodium layer in 1969 to 1970 was narrower in summertime, causing the sodium density to decrease well above the typical altitude of the ozone peak. This comparison cannot be pursued further at this time, because we do not have complete midlatitude information describing the peak of the winter sodium layer. It is suggested by available data that the seasonal variability of the total abundance of sodium may be more pronounced near solar maximum. Other characteristics of the sodium and ozone layers identified near solar minimum would persist at solar maximum, and layer interactions would lead to the nightglow profiles we observed.

As a final note, the very narrow layers that we observe in equatorial regions could yet prove to be an equatorial effect, as opposed to a summer-winter effect. Our data are somewhat ambiguous on this point. It will be important to further access diurnal and latitudinal effects, particularly with regard to any mismatch of density maxima. Detailed experimental photometric and lidar studies will be necessary to determine how and where a mismatch of the ozone and sodium density profiles may change the profile shape of Na-D emissions.

REFERENCES

- Ager, J. W. III, C. L. Talcott, and C. J. Howard, "Gas phase kinetics of the reactions of Na and NaO with O₃ and N₂O," J. Chem. Phys., **85**, 5584-5592, 1986.
- Barth, C. A., D. W. Rusch, R. D. Thomas, G. H. Mount, G. J. Rottman, G. E. Thomas, R. W. Sanders, and G. M. Lawrence, "Solar mesosphere explorer: scientific objectives and results," Geophys. Res. Lett., **10**, 237-240, 1983.
- Batista, P. P., B. R. Clemesha, D. M. Simonich, and V. W. J. H. Kirchhoff, "Tidal oscillations in the atmospheric sodium layer," J. Geophys. Res., **90**, 3881-3888, 1985.
- Blamont, J. E., and T. M. Donahue, "Sodium dayglow: observation and interpretation of a large diurnal variation," J. Geophys. Res., **69**, 4097-4127, 1964.
- Clemesha, B. R., V. W. J. H. Kirchhoff, and D. M. Simonich, "Simultaneous observations of the Na 5893-Å nightglow and the distribution of sodium atoms in the mesosphere," J. Geophys. Res., **83**, 2499-2503, 1978.
- Dobson, G. M. B., Exploring the Atmosphere, Clarendon Press, Oxford, 1968.
- Donahue, T. M. and J. E. Blamont, "Sodium in the upper atmosphere," Ann. Geophys., **17**, 116-133, 1961.
- Evans, W. F. J., D. M. Hunten, E. J. Llewellyn, and A. V. Jones, "Altitude profile of the infrared atmospheric system of oxygen in the dayglow," J. Geophys. Res., **73**, 2885, 1968.
- Gardner, C. S., D. G. Voelz, C. R. Philbrick, and D. P. Sipler, "Simultaneous lidar measurements of the sodium layer at the Air Force Geophysics Laboratory and the University of Illinois," J. Geophys. Res., **91**, 12131-12136, 1986a.
- Gardner, C. S., D. G. Voelz, C. F. Sechrist, and A. C. Segal, "Lidar studies of the nighttime sodium layer over Urbana, Illinois. 1. Seasonal and nocturnal variations," J. Geophys. Res., **91**, 13659-13673, 1986b.
- Gibson, A. J., and M. C. W. Sandford, "The seasonal variation of the night-time sodium layer," J. Atmos. Terr. Phys., **33**, 1675-1684, 1971.
- Green, B. D., W. T. Rawlins, and R. M. Nadile, "Diurnal variability of vibrationally excited mesospheric Na as observed during the SPIRE mission," J. Geophys. Res., **91**, 311-320, 1986.
- Hays, P. B., and R. G. Roble, "Observations of mesospheric ozone at low latitudes," Planet. Space Sci., **21**, 273-279, 1973.

- Hingane, L. S., "Ozone in the mesosphere and lower thermosphere," Proc. Indian Acad. Sci., **93**, 91-103, 1984.
- Hunten, D. M., A. V. Jones, C. D. Ellyett, and E. C. McLauchlan, "Sodium twilight at Christchurch, New Zealand," J. Atmos. Terr. Phys., **26**, 67-76, 1964.
- Hunten, D. M., "A meteor-ablation model of the sodium and potassium layers," Space Science Rev., **6**, 493-573, 1967.
- Jegou, J. P., C. Granier, M.L. Chanin, and G. Megie, "General theory of the alkali metals present in the earth's upper atmosphere. I. Flux model: chemical and dynamical processes," Ann. Geophys., **3**, 163-176, 1985a.
- Jegou, J. P., C. Granier, M.L. Chanin, and G. Megie, "General theory of the alkali metals present in the earth's upper atmosphere. II. Seasonal and meridional variations," Ann. Geophys., **3**, 299-312, 1985b.
- Kirchhoff, V. W. J. H., B. R. Clemesha, and D. M. Simonich, "Sodium nightglow measurements and implications on the sodium photochemistry," J. Geophys. Res., **84**, 1324-1327, 1979.
- Kirchhoff, V. W. J. H., B. R. Clemesha, and D. M. Simonich, "Seasonal variation of ozone in the mesosphere," J. Geophys. Res., **86**, 1463-1466, 1981a.
- Kirchhoff, V. W. J. H., B. R. Clemesha, and D. M. Simonich, "The atmospheric neutral sodium layer 1. Recent modeling compared to measurements," J. Geophys. Res., **86**, 6892-6898, 1981b.
- Kirchhoff, V. W. J. H., and B. R. Clemesha, "The atmospheric neutral sodium layer 2. Diurnal variations," J. Geophys. Res., **88**, 442-450, 1983.
- Kolb, C. E., and J. B. Elgin, "Gas phase chemical kinetics of sodium in the upper atmosphere," Nature, London., **263**, 488-489, 1976.
- London, J., "Radiative energy sources and sinks in the stratosphere and mesosphere," pp. 703-721, in: Nicolet, M., and A. C. Aikin (eds.), Proceedings of the Nato Advanced Study Institute on Atmospheric Ozone: Its Variation and Human Influences, U. S. Department of Transportation, Washington, DC, 1980.
- Megie, G., and J. E. Blamont, "Laser sounding of atmospheric sodium interpretation in terms of global atmospheric parameters," Planet. Space Sci., **25**, 1093-1109, 1977.
- Megie, G., F. Bos, J. E. Blamont, and M. L. Chanin, "Simultaneous nighttime lidar measurements of atmospheric sodium and potassium," Planet. Space Sci., **26**, 27-35, 1978a.
- Megie, G., M. L. Chanin, G. Y. Toulinov, and Y.P. Doudoladov, "High latitude measurements of the atomic sodium concentration and neutral temperature at the mesopause level by the lidar technique," Planet. Space Sci., **26**, 509-511, 1978b.
- Pranke, J. B., A. B. Christensen, F. A. Morse, D. R. Hickman, W. T. Chater, C. K. Howey, and D. A. Jones, "A satellite-borne limb scanning ultraviolet spectrometer for thermospheric remote sensing," Appl. Opt., **21**, 3941-3952, 1982.

- Rees, M. H., G. J. Romick, and A. E. Belon, "The intensity of the sodium-D lines in the auroral zone," Ann. Geophys., **31**, 311-320, 1975.
- Shelton, J. D., and C. S. Gardner, "Theoretical and lidar studies of the density response of the mesospheric sodium layer to gravity wave perturbation," Aeron. Rep. 99, University of Illinois, Urbana, 1981.
- Silver, J. A., and C. E. Kolb, "Determination of the absolute rate constants for the room temperature reactions of atomic sodium with ozone and nitrous oxide," J. Phys. Chem., **90**, 3263-3266, 1986.
- Simonich, D. M., B. R. Clemesha, and V. W. J. H. Kirchhoff, "Mesospheric sodium layer at 23 S: nocturnal and seasonal variation," J. Geophys. Res., **84**, 1543-1550, 1979.
- Sipler, D. P., and M. A. Biondi, "Evidence for chemiexcitation as the source of the sodium nightglow," Geophys. Res. Lett., **2**, 106-108, 1975.
- Smith, L. L., and W. R. Steiger, "Night airglow intensity variations in the [OI] 5577 Å, [OI] 6300 Å, and [NaI]5890-5896 Å emission lines," J. Geophys. Res., **73**, 2531-2538, 1968.
- Solomon, S., D. W. Rusch, R. J. Thomas, and R. S. Eckman, "Comparison of mesospheric ozone abundances measured by the Solar Mesosphere Explorer and model calculations," Geophys. Res. Lett., **10**, 249-252, 1983.
- Sullivan, H. M., "Seasonal variation of the twilight sodium layer," J. Atmos. Terr. Phys., **33**, 573-579, 1971.
- Swider, W., "Sodium Nightglow: chemically independent of sodium content," J. Geophys. Res., **91**, 6742-6746, 1986a.
- Swider, W., "Mesospheric sodium: implications using a steady-state model," Planet. Space Sci., **34**, 603-608, 1986b.
- Thomas, R. J., C. A. Barth, G. J. Rottman, D. W. Rusch, G. H. Mount, G. M. Lawrence, R. W. Sanders, G. E. Thomas, and L. E. Clemens, "Ozone density distributions in the mesosphere (50-90 km) measured by the SME limb scanning near infrared spectrometer," Geophys. Res. Lett., **10**, 245-248, 1983.
- Thomas, R. J., C. A. Barth, and S. Solomon, "Seasonal variations of ozone in the upper mesosphere and gravity waves," Geophys. Res. Lett., **11**, 673-676, 1984.

LABORATORY OPERATIONS

The Aerospace Corporation functions as an "architect-engineer" for national security projects, specializing in advanced military space systems. Providing research support, the corporation's Laboratory Operations conducts experimental and theoretical investigations that focus on the application of scientific and technical advances to such systems. Vital to the success of these investigations is the technical staff's wide-ranging expertise and its ability to stay current with new developments. This expertise is enhanced by a research program aimed at dealing with the many problems associated with rapidly evolving space systems. Contributing their capabilities to the research effort are these individual laboratories:

Aerophysics Laboratory: Launch vehicle and reentry fluid mechanics, heat transfer and flight dynamics; chemical and electric propulsion, propellant chemistry, chemical dynamics, environmental chemistry, trace detection; spacecraft structural mechanics, contamination, thermal and structural control; high temperature thermomechanics, gas kinetics and radiation; cw and pulsed chemical and excimer laser development including chemical kinetics, spectroscopy, optical resonators, beam control, atmospheric propagation, laser effects and countermeasures.

Chemistry and Physics Laboratory: Atmospheric chemical reactions, atmospheric optics, light scattering, state-specific chemical reactions and radiative signatures of missile plumes, sensor out-of-field-of-view rejection, applied laser spectroscopy, laser chemistry, laser optoelectronics, solar cell physics, battery electrochemistry, space vacuum and radiation effects on materials, lubrication and surface phenomena, thermionic emission, photo-sensitive materials and detectors, atomic frequency standards, and environmental chemistry.

Computer Science Laboratory: Program verification, program translation, performance-sensitive system design, distributed architectures for spaceborne computers, fault-tolerant computer systems, artificial intelligence, micro-electronics applications, communication protocols, and computer security.

Electronics Research Laboratory: Microelectronics, solid-state device physics, compound semiconductors, radiation hardening; electro-optics, quantum electronics, solid-state lasers, optical propagation and communications; microwave semiconductor devices, microwave/millimeter wave measurements, diagnostics and radiometry, microwave/millimeter wave thermionic devices; atomic time and frequency standards; antennas, rf systems, electromagnetic propagation phenomena, space communication systems.

Materials Sciences Laboratory: Development of new materials: metals, alloys, ceramics, polymers and their composites, and new forms of carbon; non-destructive evaluation, component failure analysis and reliability; fracture mechanics and stress corrosion; analysis and evaluation of materials at cryogenic and elevated temperatures as well as in space and enemy-induced environments.

Space Sciences Laboratory: Magnetospheric, auroral and cosmic ray physics, wave-particle interactions, magnetospheric plasma waves; atmospheric and ionospheric physics, density and composition of the upper atmosphere, remote sensing using atmospheric radiation; solar physics, infrared astronomy, infrared signature analysis; effects of solar activity, magnetic storms and nuclear explosions on the earth's atmosphere, ionosphere and magnetosphere; effects of electromagnetic and particulate radiations on space systems; space instrumentation.